J Electroceram (2011) 27:162–168
DOI 10.1007/s10832-011-9661-8

Photoluminescence and Raman spectroscopy characterization of highly c-axis oriented $Mg_xZn_{1-x}O$ thin films on Pt-coated silicon substrates

Xinman Chen · Hong Zhou · Guangheng Wu · Dinghua Bao

Received: 19 April 2011 / Accepted: 27 October 2011 / Published online: 15 November 2011

Abstract Highly c-axis oriented $Mg_xZn_{1-x}O(x = 0 \sim 0.2)$ thin films with pure hexagonal phase were prepared on Pt/TiO_2/SiO_2/Si substrates by chemical solution deposition method, and their structure, photoluminescence, and lattice vibrational properties were studied. For the thin films with Mg contents ranging $0 \leq x \leq 0.20$, the room-temperature near-band-edge emission exhibited blueshift up to about 0.35 eV, indicating that the band-gaps of thin films could be tailored by Mg incorporation, meanwhile, the green emission of the thin films enhanced with increasing Mg content. Raman spectra analysis indicated that the decreasing high frequency E_2 Raman modes showed composition-dependent asymmetrically broadening. The difference of electronegativity between Mg^{2+} for Zn^{2+} as well as the potential fluctuation were discussed. Furthermore, longtitudial optical modes exhibited one-mode behavior with observed ~25.8 cm^{-1} blueshift. X-ray photoelectron spectroscopy measurements clearly confirmed the Mg incorporation.

Keywords MgZnO · Sol-gel · Raman spectroscopy · C-axis orientation

PACS 63.20.D- · 68.60.Wm · 78.55.Et · 81.15.Lm

X. Chen
Institute of Opto-electronic Materials and Technology,
South China Normal University,
Guangzhou 510631, People's Republic of China

X. Chen · H. Zhou · G. Wu · D. Bao (✉)
State Key Laboratory of Optoelectronic Materials and Technologies, School of Physics and Engineering,
Sun Yat-Sen University,
Guangzhou 510275, People's Republic of China
e-mail: stsbdh@mail.sysu.edu.cn

1 Introduction

Zinc magnesium oxide ($Mg_xZn_{1-x}O$) thin films, with 3.37~7.8 eV band-gap, have attracted much attention for their ultraviolet (UV) light emitting and laser device applications at room temperature [1–3]. Usually, these $Mg_xZn_{1-x}O$ thin films were prepared on silicon, sapphire, and fused silica substrates by various preparation methods. To improve the optoelectronic properties of $Mg_xZn_{1-x}O$ thin films, low lattice mismatch between substrates and films is required. It was noted that platinum (Pt) shows low mismatch (1.4%) between Pt (111) plane and c-plane of ZnO [4], and better crystal quality and performance of ZnO thin films were reported previously with Pt layers acting as buffer layer between film and silicon substrate. Yamada et al. reported on the improvement of the crystal quality and effective electromechanical coupling coefficient for ZnO thin films on Pt/Al bottom electrode [4]. Duclère and coworkers have reported that ZnO thin films on Pt buffer layers exhibited strong free exciton resonances with little damping at low temperature [5].

Additionally, Pt is a good candidate for conductive electrode, facilitating the fabrication of some devices. Lately, our investigations showed that the $Mg_xZn_{1-x}O$ thin films on Pt/Ti/SiO_2/Si substrates exhibit the excellent resistance switching effect, which can be used in nonvolatile resistance memories [6, 7]. However, these optoelectronic properties of $Mg_xZn_{1-x}O$ films correlate with their structure and vibration behaviors of sublattice. Therefore, further study of $Mg_xZn_{1-x}O$ films prepared on Pt/TiO_2/SiO_2/Si substrates is required.

In this study, $Mg_xZn_{1-x}O$ thin films were prepared on Pt/TiO_2/SiO_2/Si substrates by chemical solution deposition method. The structure and photoluminescent properties as well as the lattice vibrational behaviors of the thin films were studied.

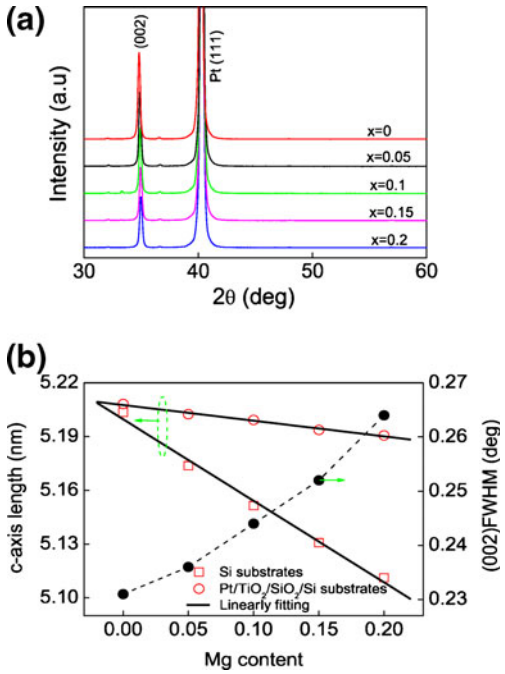

Fig. 1 (**a**) XRD patterns of $Mg_xZn_{1-x}O$ thin films on $Pt/TiO_2/SiO_2/Si$ substrates with different Mg content. (**b**) Mg composition dependence of c-axis length and FWHM of $Mg_xZn_{1-x}O$ thin films on $Pt/TiO_2/SiO_2/Si$ substrates. The solid straight line in (**b**) is linearly fitting results of calculated c-axis length: c(Å)=5.203-0.455x and c(Å)=5.208-0.009x on Si and $Pt/TiO_2/SiO_2/Si$ substrates, respectively

2 Experimental procedure

The $Mg_xZn_{1-x}O$ $(x = 0 \sim 0.20)$ thin films were fabricated by chemical solution deposition method. The $Mg_xZn_{1-x}O$ solutions with different Mg contents were synthesized using zinc acetate dihydrate ($Zn(CH_3COO)_2{\cdot}2H_2O$) and magnesium acetate tetrahydrate ($Mg(CH_3COO)_2{\cdot}4H_2O$) as source materials. In brief, the two source materials were dissolved in the mixing solution of 2-methoxyethanol and diethanolamine (DEA). The mixture above was kept at 80°C for 2 h with continuing stirring. Homogeneous and transparent solutions were obtained after cooling to room temperature. The concentrations of metal ions in all the solutions were adjusted to 0.5 mol/L.

The $Mg_xZn_{1-x}O$ solutions were deposited onto $Pt/TiO_2/SiO_2/Si$ substrates by using a spinner operated at 2500 rpm for 20 s. The wet films obtained were dried at 350°C for 5 min to remove the solvent and organic residuals. The procedures above were repeated until the desired thickness of the films was achieved. Then, the thin films were annealed at 650°C for 1 h. In present study, thickness of the thin films was about 350 nm.

The structure of the thin films was characterized by a Rigaku (D-MAX 2200 VPC) x-ray diffractometer (XRD) with Cu K_α radiation (λ=0.154 nm) while the working current and voltage were 30 mA and 40 kV respectively. The glancing-incidence XRD (GIXRD) method was employed to detect the cubic (200) phase segregation, and the incident angle was fixed at 1.5°. The surface morphology was characterized by the S-4800 scanning electron microscopy (SEM, Hitachi).

The photoluminescence (PL) spectra at room temperature were measured by RF-5301PC (Shimadzu, Japan) spectrofluorophotometer using Xe lamp. The excitation wavelength was 325 nm. The micro-Raman spectrometer (Renishaw, U.K) was employed to investigate the lattice vibrational behaviors of the thin films at room temperature. To avoid the heating effect and resonant effect, the nonresonant Raman spectra were characterized with the visible excitation laser (λ=514.5 nm). In addition, the chemical states of the $Mg_xZn_{1-x}O$ films were investigate by X-ray photoelectron spectroscopy (XPS) using ESCA-Lab250 (U.K) spectrometer with monochromatic Al K_α radiation ($h\nu$=1486 eV). All binding energies were calibrated with respect to C1s spectral line at 284.8 eV.

3 Results and discussion

3.1 Phase structure, c-axis oriented growth and microstructure

Figure 1(a) shows XRD patterns of pure ZnO and $Mg_xZn_{1-x}O$ thin films with different Mg contents (x=0.05, 0.1, 0.15, and 0.2, respectively) on $Pt(111)/TiO_2/SiO_2/Si$ substrates. The sharp and strong (002) peaks appear in all the thin film samples, suggesting that the thin films are highly (002) preferentially oriented. This can be attributed to the combination of the lowest surface energy of (002) plane with the small mismatch (1.4%) between the c plane of the thin films and Pt (111) plane [4, 5]. Meanwhile, the intensities of (002) peaks decrease as Mg content increases. Generally, $Mg_xZn_{1-x}O$ with the Mg content beyond 4% was supposed to be not thermodynamically stable, however, the solubility limit of Mg in ZnO lattice correlates with the growth mechanisms as well as condition employed. [3, 8] To further identify the effect of Mg content on phase structure of $Mg_xZn_{1-x}O$ films, GIXRD method has been employed, which confirmed that the films remain pure hexagonal structure without cubic phase segregation when $x \leq 0.2$.

From the XRD data, the c-axis lattice parameters of the thin films and FWHM of (002) peaks as a function of Mg content can be obtained as shown in Fig. 1 (b). The FWHM of (002) peaks increases with increasing Mg content. The calculated c-axis lattice constants of hexagonal structure decrease linearly from 0.5208 nm to 0.5191 nm with Mg contents from 0 to 0.2. Therefore, the shortening c-axis lattice and broadening (002) FWHM indicate successful incorporation of Mg into ZnO lattice due to the different

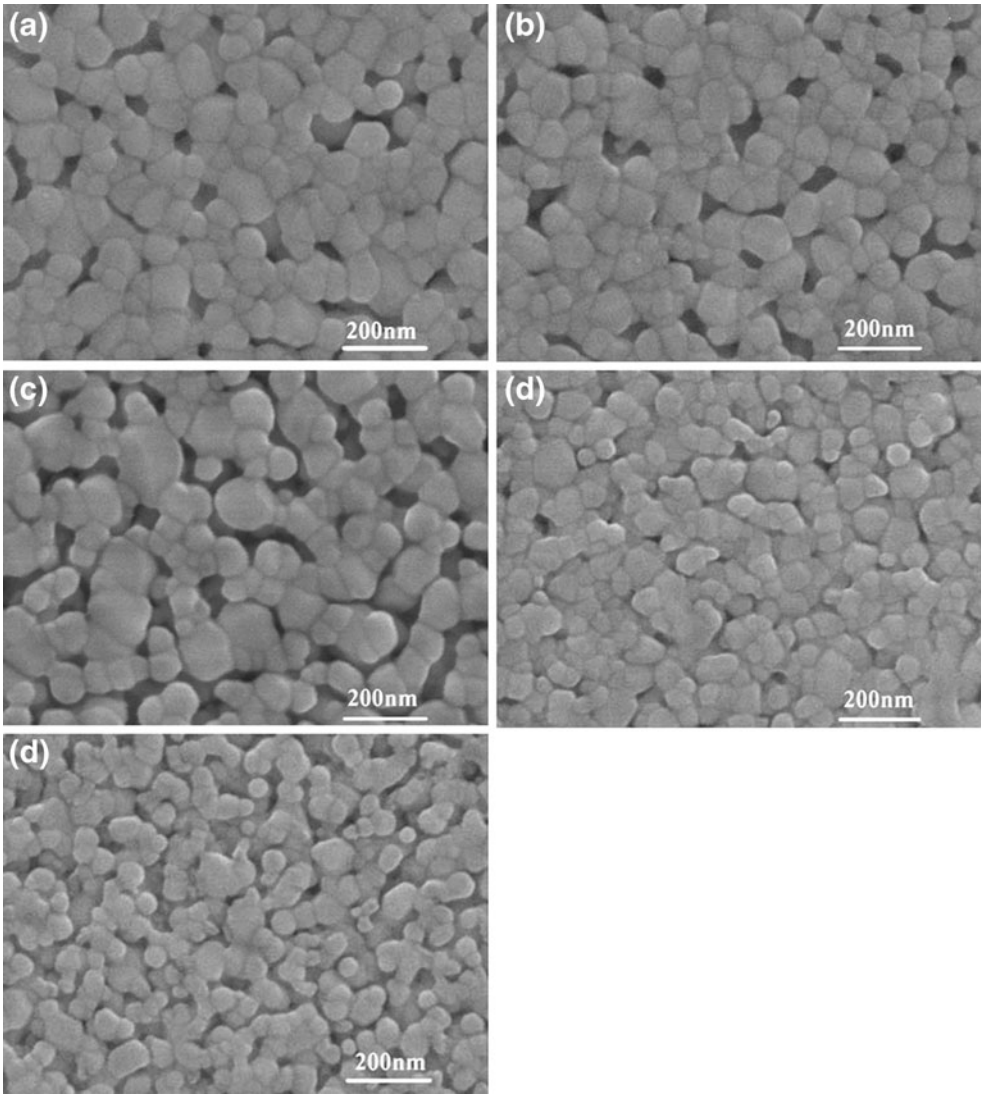

Fig. 2 SEM images of $Mg_xZn_{1-x}O$ films on $Pt/TiO_2/SiO_2/Si$ substrates. (**a**) x=0; (**b**) x=0.005; (**c**) x=0.1; (**d**) x=0.15; (**e**) x=0.2

radii of Zn^{2+} ion (0.6 Å) and Mg^{2+} ion (0.57 Å) [3, 9, 10]. It is worth noting that the extent to decrease of c-axis lattice due to Mg incorporation is smaller than previous reports [3, 4]. For comparison, the c-axis length of $Mg_xZn_{1-x}O$ films on Si substrates was shown in Fig 1 (b). Obviously, the c-axis length of $Mg_xZn_{1-x}O$ films on $Pt/TiO_2/SiO_2/Si$ substrates decreases smaller than that on Si substrates due to the negligible strain caused by well

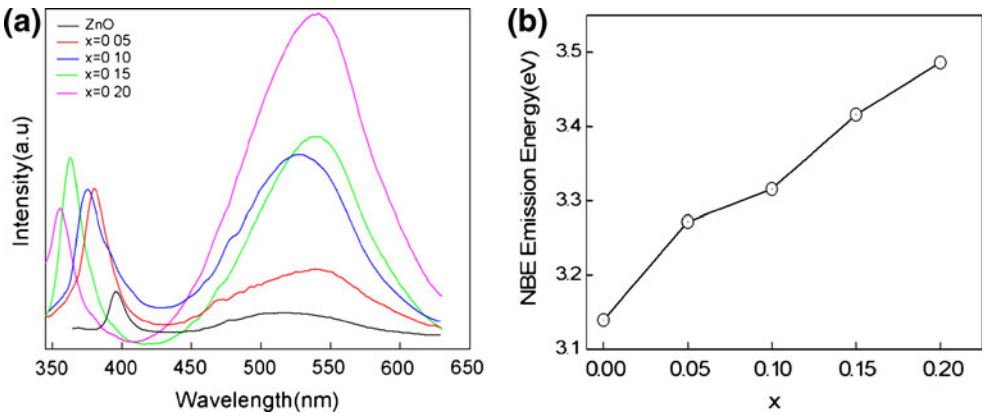

Fig. 3 (**a**) Room-temperature PL spectra of pure ZnO and $Mg_xZn_{1-x}O$ thin films; (**b**) Near-band-edge energy of PL spectra plotted as x

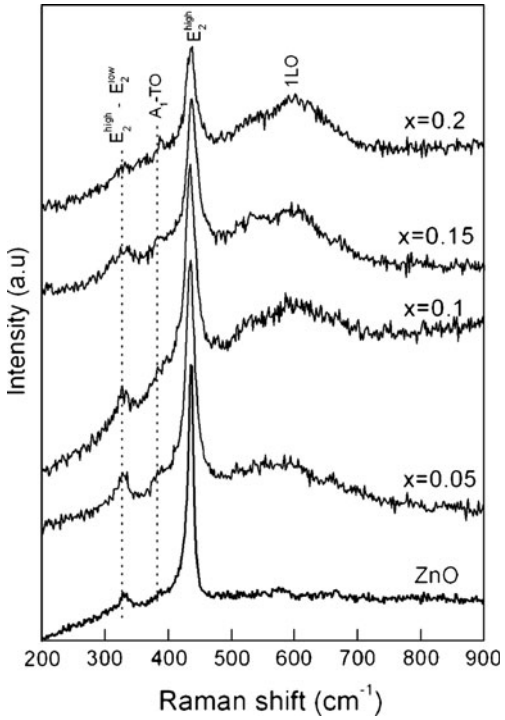

Fig. 4 Raman spectra of pure ZnO thin films and $Mg_xZn_{1-x}O$ (x= 0.05, 0.1, 0.15, and 0.2) thin films on $Pt/TiO_2/SiO_2/Si$ substrates at room temperature

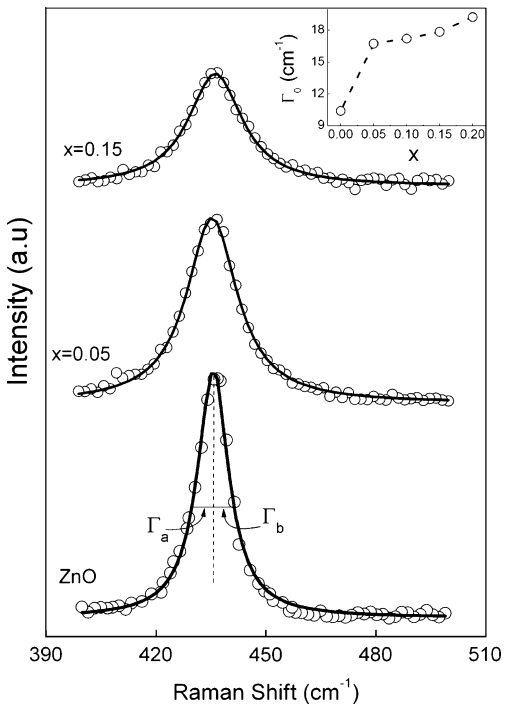

Fig. 5 The E_2^{high} modes of ZnO and $Mg_xZn_{1-x}O$ thin films with x= 0.05 and 0.15. The solid lines present the Lorentzian fitting of experimental data (square). The inset shows the change of Lorentzian linewidth $\Gamma_0=(\Gamma_a+\Gamma_b)$ as function of x

lattice-matching between Pt (111) and the films. Figure 2 shows the typical surface SEM images of $Mg_xZn_{1-x}O$ films on $Pt/TiO_2/SiO_2/Si$ substrates. The smooth surface morphology can be observed with some pores but well-distributed fine grains. The grain size decreases with the increasing Mg content in $Mg_xZn_{1-x}O$ films, originating from the formatin MgO clusters surrounding the crystalline $Mg_xZn_{1-x}O$ [10].

3.2 Photoluminescent property

Figure 3 (a) shows room temperature photoluminescence (PL) spectra of $Mg_xZn_{1-x}O(x = 0 \sim 0.2)$ thin films on $Pt/TiO_2/SiO_2/Si$ substrates by chemical solution deposition. The near-band-edge (NBE) UV emission as well as green emission can be observed clearly. The NBE emission energy as a function of Mg content is shown as Fig. 3(b). The NBE energy exhibits ~0.35 eV blueshift as Mg content increases from 0 up to 0.2, suggesting the broadening band-gap of $Mg_xZn_{1-x}O$ thin films.

Moreover, compared with ZnO thin films, the intensity of NBE emission and green peaks enhances significantly due to Mg incorporation. Generally, the NBE emission is attributed to the radiative recombination of the free exciton, while the green emission is related with the intrinsic defects of films [1–3]. It was reported that the incorporation of Mg atom into ZnO lattice can decrease the concentration of oxygen-vacancy-related nonradiative defects during post-heating process due to the stronger coalescence with oxygen atoms, which can enhance the intensities of NBE emission [11, 12]. However, the NBE emission intensity decreases while the green emission boosts up when x=0.2. It is reasonable that excessive Mg incorporation into ZnO can cause the increase of nonradiative recombination lifetime and recreate the structure-related defects like disorders and boundaries, deteriorating the films quality. Theses factors can result in the intensifying deep level luminescence and depression of the photoluminescence of NBE peaks [9, 11].

3.3 Raman spectroscopy characterization

Figure 4 shows Raman spectra (200~900 cm^{-1}) of the $Mg_xZn_{1-x}O(x = 0 \sim 0.2)$ thin films deposited on $Pt/TiO_2/SiO_2/Si$ substrates, from which the effect of Mg doping levels on vibrational properties of ZnO lattice has been investigated. In Fig. 4, the sharp high-frequency E_2 modes (E_2^{high}), fist-order longitudinal optical modes (1LO) can be observed clearly. Two weak peaks at ~330 cm^{-1} and ~385 cm^{-1} can be attributed to the multiple phonon (MP) processes (E_2^{high}-E_2^{low}) and A_1-TO mode, respectively [13, 14].

The E_2^{high} peaks, which are associated with motion of O^{2-} ions, are characteristic of hexagonal structure of ZnO

Table 1 Raman peak parameters of E_2^{high} and 1LO modes of $Mg_xZn_{1-x}O$ thin films

x	E_2^{high}			1LO
	Peak position (cm^{-1})	$\Gamma_0=(\Gamma_a+\Gamma_b)$ (cm^{-1})	Γ_a/Γ_b	Peak position (cm^{-1})
0	435.4	10.40	1.04	575.4
0.05	435.6	16.76	0.90	582.7
0.1	436.2	17.22	0.85	587.7
0.15	436.9	17.87	0.81	594.4
0.20	437.5	19.26	0.79	601.2

[13–16]. Therefore, the hexagonal structure of $Mg_xZn_{1-x}O$ ($x = 0 \sim 0.2$) films can be confirmed from Raman spectra. To clarify the effect of Mg doping on lattice structure, the E_2^{high} peaks of $Mg_xZn_{1-x}O(x = 0,\ 0.05,\ 0.15)$ films were Lorentzian fitted as Fig. 5. The corresponding asymmetry factor was defined as Γ_a/Γ_b, and the FWHM of E_2^{high} peaks (Γ_0) can be described as $\Gamma_0=\Gamma_a+\Gamma_b$. As seen from Fig. 4, the intensity of the dominant E_2^{high} peaks decreases with increasing Mg content, while Lorentzian-lineshape broadenes asymmetrically. Compositional dependence of the E_2^{high} and 1LO on Mg content is listed as Table 1.

Although the ionic radii of Zn^{2+} and Mg^{2+} ions are similar, it is noted that Mg^{2+} is more electronegative than Zn^{2+}, and this result in great discrepancy of bond character between the Mg-O and Zn-O. The Mg-O bond shows more ionicity than Zn-O bond, while the bond energies of Mg-O and Zn-O are ~373.7 kJ/mol and ~284.1 kJ/mol, respectively [17]. Substitution of Zn^{2+} by Mg^{2+} causes the formation of Mg-O bond, restricting or reducing the motion of O^{2-} of lattice, and decreasing the intensity of E_2^{high} peaks accordingly. In addition, it is acceptable that potential fluctuation and the local lattice disorder can be resulted in inevitably by the replacement of Mg^{2+} for Zn^{2+} due to the difference of their electronegativity, which can distort and broaden the spectra lineshape [16, 18]. Both factors depend on the distribution of Mg^{2+} in the crystals. Accordingly, more potential fluctuation and lattice disorder can be caused due to more composition non-uniformity when Mg content increases [19]. It is the lattice disorders that enhance the emission of nonradiative recombination and suppress the NBE when Mg content exceeds 0.15.

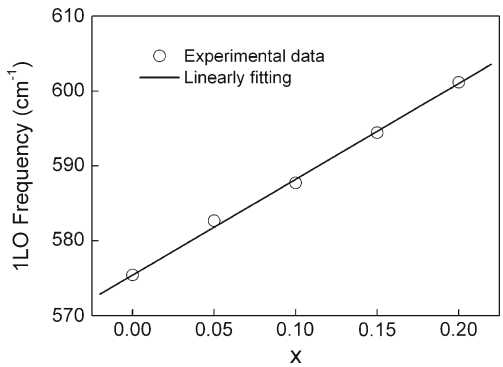

Fig. 6 Dependence of 1LO phonon frequencies of $Mg_xZn_{1-x}O$ alloy films on Mg content. The fitting result (solid line) shows: $\omega-_{1LO}(x,\ cm^{-1}) = 575.4 + x*128(\pm 3.18)$

In ZnO-based semiconductors, behavior of the polar 1LO mode is also important because the optoelectronic performance of devices can be modified by it through Fröhlich interaction [13, 14]. As can be seen in Fig. 4, in all hexagonal $Mg_xZn_{1-x}O$ films, 1LO mode only exhibits ZnO-like "one-mode" behavior, which can be well explained by modified random-element-isodisplacement (MREI) mode. In $Mg_xZn_{1-x}O$ crystal, the mass (m) of substituting atom is larger than the reduced mass (μ) of compounds: $m_{Zn} = 65 > \mu_{MgO} = 9.6$, $m_{Mg} = 24 > \mu_{ZnO} = 12.8$.[20] 1LO modes of $Mg_xZn_{1-x}O$ films on $Pt/TiO_2/SiO_2/Si$ substrates are compositionally dependent, as shown in Table 1 and Fig. 6. And 1LO mode shifts toward high frequency from 575.4 to 601.2 cm^{-1} as Mg content increases to 0.2, a blueshift of about 25.8 cm^{-1} occurs. Based on the MREI mode, the experimental data can be simply expressed as a linear function of x ($0 \le x \le 0.2$): $\omega-_{1LO}(x,\ cm^{-1}) = 575.4 + x*128(\pm 3.18)$. The blueshift of 1LO modes reflects the strained Zn-O bonds due to the Mg doping.

3.4 XPS characterization

The x-ray photoelectron spectra (XPS) were employed to understand the change of chemical states after Mg incorporation into ZnO lattice. High-resolution XPS of Mg2p, Zn2p and O1s of ZnO and $Mg_{0.2}Zn_{0.8}O$ films are shown in Fig. 7. The Mg2p peak presents two components at 49.5 eV and 50.3 eV, which are attributed to the $Mg2p_{3/2}$ and $Mg2p_{1/2}$, respectively. The shifts of binding energy compared with that of Mg element, suggests successful incorporation of Mg. In the high-resolution spectra of Zn2p of ZnO sample, shown in Fig. 7(b), two peaks at 1021.02 eV and 1044.08 eV correspond to $Zn2p_{3/2}$ and $Zn2p_{1/2}$ with a 23.06 eV gap between them. While in $Mg_{0.2}Zn_{0.8}O$ sample, $Zn2p_{3/2}$ peak positively shift to1021.92 eV with a 23.25 eV gap from $Zn2p_{1/2}$. The binding energy shift of $Zn2p_{3/2}$ peaks and change of the gap confirm the variation of chemical states of

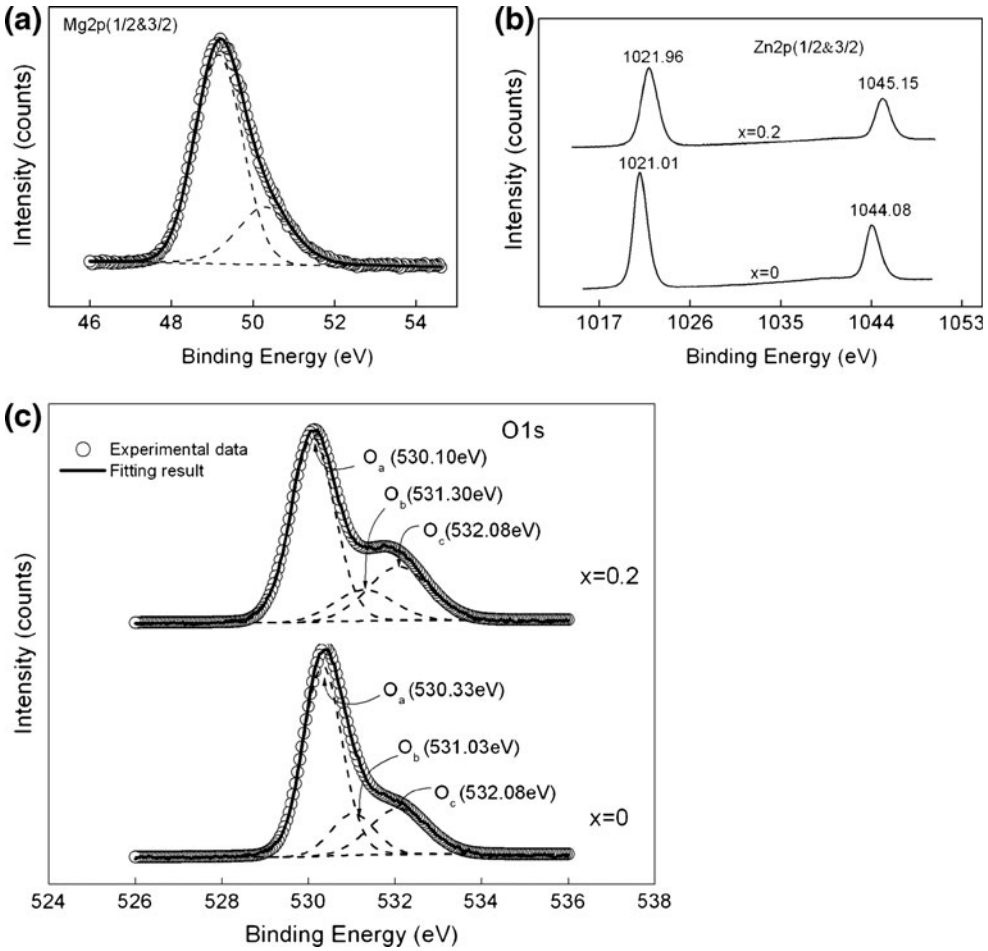

Fig. 7 XPS of ZnO and $Mg_xZn_{1-x}O$ (x=0.2) films: (**a**) Mg2p, (**b**) Zn2p, and (**c**) O1s spectra deconvoluted by Lorentzian fitting. The solid lines are fitting results while the dashed lines are component peaks

Zn^{2+}, which can be related with the formation of ternary $Mg_{0.2}Zn_{0.8}O$ alloy crystals.

Figure 7(c) shows the deconvoluted O1s XPS spectra. The fitting results (green curve) agree with the experimental data well. In ZnO sample, the three components are at 530.33 eV, 531.03 eV, and 532.08 eV, respectively. The high binding energy peak at 532.08 eV is related to chemisorbed oxygen species of the surface of ZnO film due to the exposure to atmosphere. The 530.33 eV peak is assigned to lattice O^{2-} ions while the medium binding energy peak located at 531.03 eV is associated with O^{2-} ions in the oxygen deficient regions within the matrix of ZnO. [21, 22] While the O1s spectra of $Mg_{0.2}Zn_{0.8}O$ film can also be resolved into three peaks at 530.10 eV, 531.3 eV, 532.08 eV which are ascribed to O1s in Mg-O-Zn, defective state and chemisorbed oxygen species respectively. Compared with ZnO, 0.23 eV redshift of binding energy in lattice oxygen, with 0.27 eV blueshift in defective state oxygen, can be observed due to formation of $Mg_{0.2}Zn_{0.8}O$ alloy. These shifts can be resulted principally from the difference of electronegativity of Mg^{2+} and Zn^{2+} ions, which agrees with the results of Raman spectra.

4 Conclusions

Highly c -axis oriented $Mg_xZn_{1-x}O$ films were prepared on Pt (111)/TiO_2/SiO_2/Si substrates by chemical solution deposition method. The NBE emission of $Mg_xZn_{1-x}O$ films (x=0~0.2) with hexagonal structure exhibits ~0.35 eV blueshifts combined with strong green PL. Compositionally dependent nonresonant Raman spectra were investigated. Asymmetric E_2^{hig} peaks broaden and weaken with increase of Mg content. The changed electronegativity combined with potential fluctuation after substitution was discussed. While LO Raman mode of alloy films emerges as "one mode" behavior and its frequencies show incremental linear function as Mg content (x): $\omega_{-LO}(x, cm^{-1}) = 575.4 + x*128(\pm 3.18)$. Successful Mg incorporation into ZnO lattice together with resultant change of the chemical states was confirmed by XPS.

Acknowledgement The authors gratefully acknowledge support from the Natural Science Foundation of Guangdong Province, China (No. 05003289), the Specialized Research Fund for the Doctoral Program of Higher Education of China (No. 20090171110007), NSFC (Grant Nos. 50872156, 51172289, and No. U0634006), and the Natural Science Foundation of Shanghai, China (Grant No. 11ZR1426700).

References

1. Ü. Özgür, Y.I. Alivov, C. Liu, A. Teke, M.A. Reshchikov, S. Doğan, V. Avrutin, S.J. Cho, H. Morkoc, J. Appl. Phys. **98**, 041301 (2005)
2. C. Klingshirn, Chem. Phys. Chem. **8**, 782 (2007)
3. A. Ohtomo, M. Kawasaki, T. Koida, K. Masubuchi, H. Koinuma, Y. Sakurai, Y. Yoshida, T. Yasuda, Y. Segawa, Appl. Phys. Lett. **72**, 2466 (1998)
4. H. Yamada, Y. Ushimi, M. Takeuchi, Y. Yoshino, T. Makino, S. Arai, Vacuum **74**, 689 (2004)
5. J.R. Duclère, C.M. Loughlin, J. Fryar, R.O. Haire, M.G. Viry, A. Meaney, A. Perrin, E. Mcglynn, M.O. Henry, J.P. Mosnier, Thin Solid Films **500**, 78 (2006)
6. X.M. Chen, G.H. Wu, D.H. Bao, Appl. Phys. Lett. **93**, 093501 (2008)
7. X.M. Chen, G.H. Wu, W.F. Liu, P. Jiang, D.H. Bao, Appl. Phys. Lett. **94**, 033501 (2009)
8. D.Y. Jiang, D.Z. Shen, K.W. Liu, C.X. Shan, Y.M. Zhao, T. Yang, B. Yao, Y.M. Lu, J.Y. Zhang, Semcond. Sci. Technol. **23**, 035002 (2008)
9. J.F. Kong, W.Z. Shen, Y.W. Zhang, C. Yang, X.M. Li, Appl. Phys. Lett. **92**, 191910 (2008)
10. C.H. Pan, K.F. Lin, W.T. Hsu, W.F. Hsieh, J. Phys.: Condens. Matter. **19**, 186201 (2007)
11. S. Chakrabarti, S. Kar, A. Dev, S. Chaudhuri, Phys. Stat. Sol. (a) **202**, 441 (2005)
12. X.W. Zhu, Y.Q. Li, Y. Lu, L.C. Liu, Y.B. Xia, Mater. Chem. Phys. **102**, 75 (2007)
13. C. Ramon, A.L. Esther, I. Jordi, A. Luis, Phys. Rev. B **75**, 165202 (2007)
14. V.V. Ursaki, I.M. Tiginyanu, V.V. Zalamai, E.V. Rusu, G.A. Emelchenko, V.M. Masalov, E.N. Samarov, Phys. Rev. B **70**, 155204 (2004)
15. K.T. Nguyen, A. Gaur, M. Shim, Phys. Rev. Lett. **98**, 145504 (2007)
16. J. Huso, J.L. Morrison, H. Hoeck, E. Casey, L. Bergman, T.D. Pounds, M.G. Norton, Appl. Phys. Lett. **91**, 111906 (2007)
17. X. Dong, H. Zhu, B. Zhang, W. Liu, X. Li, T. Yang, G. Du, Vaccum **8**, 535 (2008)
18. L. Bergman, J.L. Morrison, X.B. Chen, J. Huso, H. Hoeck, Appl. Phys. Lett. **88**, 023103 (2006)
19. J. Chen, W.Z. Shen, N.B. Chen, D.J. Qiu, H.Z. Wu, J. Phys. Condens. Matter **15**, L475 (2003)
20. I.F. Chang, S.S. Mitra, Phys. Rev. **172**, 924 (1968)
21. X.J. Yang, X.Y. Miao, X.L. Xu, C.M. Xu, J. Xu, H.T. Liu, Opt Mater. **27**, 1602 (2005)
22. M. Chen, X. Wang, Y.H. Yu, Z.L. Pei, X.D. Bai, C. Sun, R.F. Huang, L.S. Wen, Appl. Surf. Sci. **158**, 134 (2000)